International Journal of Solids and Structures 45 (2008) 4407–4426

Contents lists available at ScienceDirect

International Journal of Solids and Structures

journal homepage: www.elsevier.com/locate/ijsolstr

Dynamic rupture of polymer–metal bilayer plates

G.J. McShane [a], C. Stewart [a], M.T. Aronson [b], H.N.G. Wadley [b], N.A. Fleck [a], V.S. Deshpande [a,*]

[a] Department of Engineering, University of Cambridge, Trumpington Street, Cambridge CB2 1PZ, UK
[b] Department of Materials Science and Engineering, University of Virginia, 116 Engineer's Way, Charlottesville, VA 22904, USA

ARTICLE INFO

Article history:
Received 20 July 2007
Received in revised form 20 March 2008
Available online 28 March 2008

Keywords:
Bilayers
Necking
Petalling
Underwater blast

ABSTRACT

Recent theoretical assessments of metal/polymer bilayers indicate a potentially significant delay in the onset of ductile failure modes, especially under dynamic loading, due to strain hardening of the polymer. The response of copper/polyurethane bilayers under dynamic and quasi-static loadings is investigated via static tensile, static bulge forming and dynamic bulge forming tests. Two polyurethanes PU1 and PU2 were chosen with a significant contrast in stiffness and ductility: PU1 has a glass transition temperature T_g close to −56 °C and at room temperature it has a low modulus, low strength and a high tensile failure strain. In contrast, PU2 has a T_g of 49 °C and at room temperature it has a high modulus and strength but a much smaller tensile failure strain. In most of the tests, the polymer coatings were approximately twice the thickness of the metal layer. Under static loadings (tensile and bulge forming) the PU2 bilayer outperformed the uncoated metal plate of equal mass while the PU1 bilayer had a performance inferior to the equivalent uncoated plate. We attribute this to the fact that the PU2 retards the necking of the copper layer and thus increases its energy absorption capacity while the PU1 coating provides no such synergistic effect. The dynamic bulge forming tests indicate that on an equal mass basis, the dynamic performance of the PU2 bilayers with a weakly bonded polymer coating were comparable to the uncoated plates but intriguingly, when the PU2 was strongly adhered to the copper plates the performance of these bilayers was inferior to that of the uncoated plates. Thus, the coatings do not provide dynamic performance benefits on an equal mass basis. However, it is shown that increasing the mass of a plate by adding a polyurethane layer can improve the performance for a given total blast impulse. Given the ease of applying polyurethane coatings they may provide a practical solution to enhancing the blast resistance of existing metallic structures.

1. Introduction

The failure of plates when subjected to dynamic loadings is of primary importance in the design of blast and ballistic resistant structures. Experiments on impulsively loaded clamped beams have revealed a range of deformation and failure modes (Menkes and Opat, 1973; Nurick and Shave, 1996). At low values of impulse I, the beams plastically bend and stretch without rupture (Mode I). At intermediate I, plate stretching is followed by tensile rupture at the supports (Mode II). And at high I, shear failure occurs at the supports with negligible plastic deformation in the remainder of the beam (Mode III). Recent theoretical studies by Lee and Wierzbicki (2005a,b) have analysed the so-called discing and petalling failure modes in impulsively loaded clamped plates. These tensile tearing modes are reminiscent of the Mode II failure modes for impulsively

* Corresponding author. Tel.: +44 1223 332664; fax: +44 1223 332662.
E-mail address: vsd@eng.cam.ac.uk (V.S. Deshpande).

0020-7683/$ - see front matter © 2008 Elsevier Ltd. All rights reserved.
doi:10.1016/j.ijsolstr.2008.03.017

loaded beams. On the other hand, Balden and Nurick (2005) have reported an experimental and numerical investigation into the so-called shear rupture modes (Mode III) of impulsively loaded clamped circular plates.

For marine structures, the pressure loading caused by the detonation of an underwater explosive is well approximated by a sharp-fronted exponentially decaying pulse (Taylor (1941)). A detailed experimental investigation by Kazemahvazi et al. (2007) found that failure modes analogous to those identified by Menkes and Opat (1973) persist for clamped circular metallic plates subjected to an underwater blast. Delaying the onset of failure of clamped monolithic or sandwiched plates subject to dynamic loading has a number of obvious practical applications and forms the motivation for the present study.

Shenoy and Freund (1999) and Guduru and Freund (2002) clearly demonstrated that material inertial effects retard tensile necking and result in the formation of multiple necks: the elongation to failure increased with the number of necks per unit length. More recently, Guduru et al. (2006) gave clear indications of the important role played by an elastomer layer in retarding necking under high strain rates. However, none of these studies accounted for material rate dependence which is known to be critical in governing the necking response of metals subjected to high rates of deformation (Hutchinson and Neale, 1977).

Following Guduru et al. (2006), Xue and Hutchinson (2007) conducted a numerical investigation into axisymmetric neck development in clamped circular metal/elastomer bilayers subject to impulsive loads. Imperfections were introduced in the plates in these calculations in order to trigger the necking of the plates. Xue and Hutchinson (2007) report substantial increases in necking limits and consequently the energy absorption capacity of these bilayers compared to uncoated metal plates of equal mass. The phenomenon is tied to the fact that they assume a neo-Hookean (non-linear elastic) relation for the elastomer so that under stretching the incremental modulus of the elastomer increases while the incremental modulus of the metal steadily decreases. Since necking instabilities are associated with reductions of the incremental modulus, necking in the bilayer is delayed to larger strains. This is illustrated by the following simple analysis. For cases where necking occurs at large strains such that elasticity can be neglected, it is adequate to approximate the uniaxial tensile stress σ versus strain ε curve of the metal by the power law relation

$$\sigma = \sigma_0 \varepsilon^N, \tag{1}$$

where σ_0 is the extrapolated flow strength at a strain of unity and N is the strain hardening exponent (Xue and Hutchinson, 2007). For simplicity, Xue and Hutchinson (2007) assumed that the tensile stress versus strain relation of the polymer is well characterised by a neo-Hookean relation of the form

$$\sigma = \frac{E}{3}\left(e^{2\varepsilon} - e^{-\varepsilon}\right), \tag{2}$$

where E is the Young's modulus of the polymer at zero strain. Now consider a bilayer comprising a metallic layer of thickness h_m and polymer layer of thickness h_p. Under plane stress ($\sigma_{33} = 0$) uniaxial straining conditions (i.e. $\varepsilon_{11} = \varepsilon, \varepsilon_{22} = 0$) the necking strain ε_n of the bilayer is given by the relation (assuming equal strain in both layers)

$$\frac{S}{4}\left(e^{2\varepsilon_n} + 3e^{-2\varepsilon_n}\right) = \left(\frac{2}{\sqrt{3}}\varepsilon_n\right)^{N-1}(\varepsilon_n - N), \tag{3}$$

where

$$S \equiv \frac{h_p E}{h_m \sigma_0}, \tag{4}$$

(Xue and Hutchinson, 2007). Note that in the limit of an uncoated metal plate ($S = 0$), Eq. (3) reduces to the classical result $\varepsilon_n = N$ indicating that necking can be delayed by increasing the strain hardening capacity of the metal. Next, consider the metal/polymer bilayer. As illustrated in Fig. 1a, ε_n increases with increasing S suggesting that increasing the thickness and/or Young's modulus of the polymer delays necking of the bilayer. Now consider uncoated and bilayer plates, each with an areal mass

$$m = \rho_m h_m + \rho_p h_p = \rho_m H_m, \tag{5}$$

where ρ_m and ρ_p are the densities of the metal and polymer, respectively, and H_m is the thickness of an uncoated metal plate with an areal mass equal to that of the bilayer. The energy absorption capacities per unit mass of the bilayer and uncoated plates (of equal mass per unit area) prior to the onset of necking are defined as $U_{bilayer}$ and $U_{monolithic}$, respectively, and are plotted in Fig. 1b as a function of h_p/h_m for the choice $N = 0.2$, $\rho_p/\rho_m = 0.15$ and selected values of E/σ_0. Significant enhancements in the energy absorption capacity on a unit mass basis are predicted by employing the bilayer construction for designs with high values of h_p/h_m and E/σ_0. To-date there have been no detailed experimental studies to substantiate or refute these predictions.

The present study aims to investigate experimentally the quasi-static and dynamic response of clamped circular copper/polyurethane bilayers. The dynamic rupture behaviour is investigated using a novel, laboratory-scale water shock tube apparatus developed by Deshpande et al. (2006). Two castable polyurethanes are considered, PU1 and PU2, with glass transition temperatures below and above room temperature, respectively. Thus, these coatings have a significant contrast in stiffness and ductility. The outline of the paper is as follows. First, the quasi-static response of copper/polyurethane bilayer plates un-

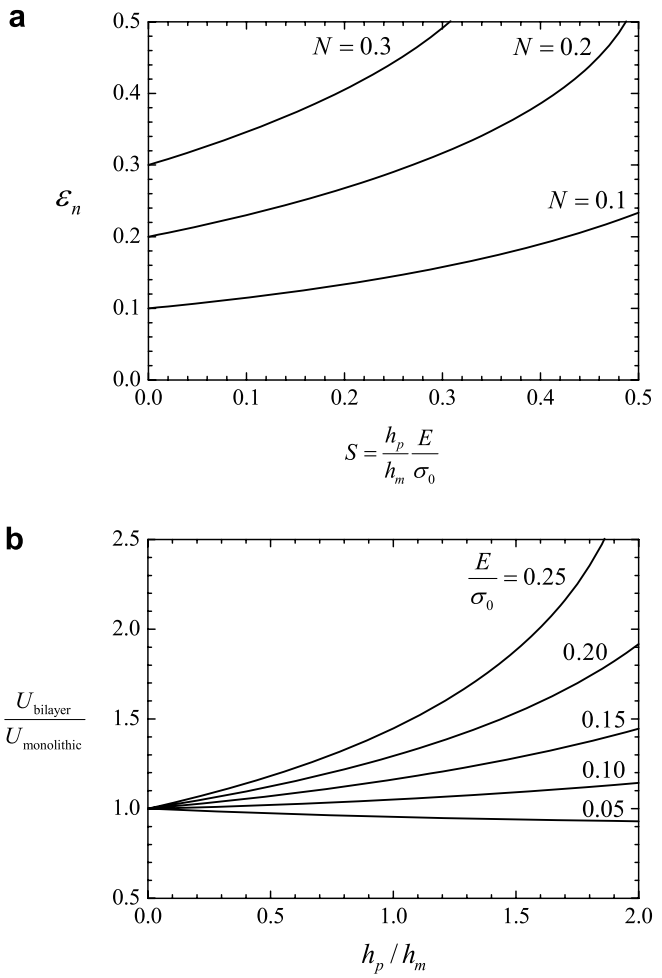

Fig. 1. Summary of the theoretical results of Xue and Hutchinson (2007) for bilayer plates under plane-strain stretching: (a) the dependence of necking strain ε_n on the non-dimensional stiffness S for three values of the metal strain hardening exponent N and (b) the ratio of energy dissipated at the onset of necking for bilayer and monolithic plates of the same mass. A range of stiffness values E/σ_0 are shown. The density ratio $\rho_p/\rho_m = 0.15$, appropriate for a copper–polyurethane bilayer.

der tensile stretching and bulge forming tests is described. Second, the dynamic response of the uncoated and bilayer plates subject to a spatially uniform load is detailed. And third, the plates are subjected to localised dynamic loading over a central patch. In all cases, the performance of the uncoated and bilayer plates is compared on an equal mass basis.

2. Characterisation of the coatings

The investigation of Xue and Hutchinson (2007) has emphasized the importance of the polymer modulus in enhancing the performance of the bilayers. In order to experimentally investigate this effect, we choose two polymers whose moduli differ by almost three orders of magnitude. In particular, we investigated two polyurethanes, designated PU1 and PU2, both with density $\rho_p \approx 1200\ \text{kg m}^{-3}$. Information pertaining to these two materials, including the manufacturer, product name, and relevant physical property information, is provided in Table 1. The glass transition temperature (T_g) of the two polyurethane polymers was determined with modulated differential scanning calorimetry (MDSC®) using a Q1000 Modulated DSC (TA Instruments–Waters, LLC). Each sample was heated over a temperature range of −80 °C to 240 °C with a heating rate of 3 °C min^{-1} and a modulation of ±0.5 °C per 60-s period. The T_g of each sample was taken to be the inflection point in the measured heat capacity versus temperature curve. Based on this definition, $T_g = -56$ °C for PU1 and $T_g = 49$ °C for PU2. At room temperature, ($T \approx 25$ °C) PU1 and PU2 are thus above and below their glass transition temperatures, respectively, and consequently PU2 has a considerably higher modulus and yield strength compared to PU1 (see Table 1). It is apparent from the information included in Table 1 that PU1 and PU2 can be used to provide coatings with a significant contrast in stiffness and ductility.

Table 1
Manufacturers' reported properties for the two polyurethane systems

Property	PU1	PU2
Manufacturer	Smooth-On (Easton, PA)	Crosslink Technology Inc. (Mississauga, ON, Canada)
Product name	PMC-780 Dry	CLC1D-078
Tensile modulus (MPa)	2.8	1120
Tensile strength (MPa)	6.2	69
Elongation to break (%)	700	16
Shore hardness	80 A	78 D

2.1. Low strain rate response

The quasi-static compressive stress versus strain curves of PU1 and PU2 for a strain rate of $\dot{\varepsilon} = 1.4 \times 10^{-4}$ s^{-1} are plotted in Fig. 2a and b, respectively. These compression tests were conducted on 6 mm × 6 mm × 6 mm cuboidal specimens in a screw-driven test machine with the specimens compressed between lubricated flat platens. The relative displacement of the platens was measured via a laser extensometer and used to define the compressive strain in the specimens while the readings from the load cell of the test machine were employed to define the stress. PU2, which is below its glass transition temperature, displays an initial elastic response followed by a distinct yield point at a stress of about 50 MPa. By contrast, PU1 displays an approximately linear response up to a nominal compressive strain of about 40% followed by a strongly softening response due to shear localisation and fragmentation within the specimen. The quasi-static peak strength of the PU1 is only about 1.4 MPa.

The quasi-static tensile response of the polymer film coatings was also measured as follows. First, bilayer plates were manufactured by applying polyurethane coatings to copper plates using a draw-down bar technique. No primer coating or pre-treatment was applied, resulting in low adhesion strength and allowing the polymer coatings to be easily peeled off the copper plates. Next, dog-bone shaped specimens were cut from these plates and the dog-bone shaped polymer coat-

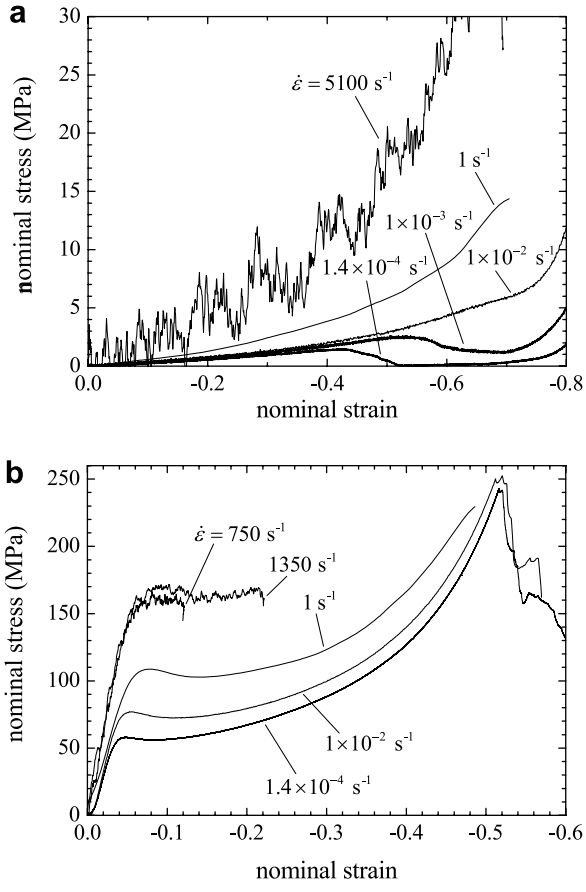

Fig. 2. Compressive properties of the polyurethane coating materials at a range of strain rates: (a) PU1 (T_g = −56 °C) and (b) PU2 (T_g = 49 °C).

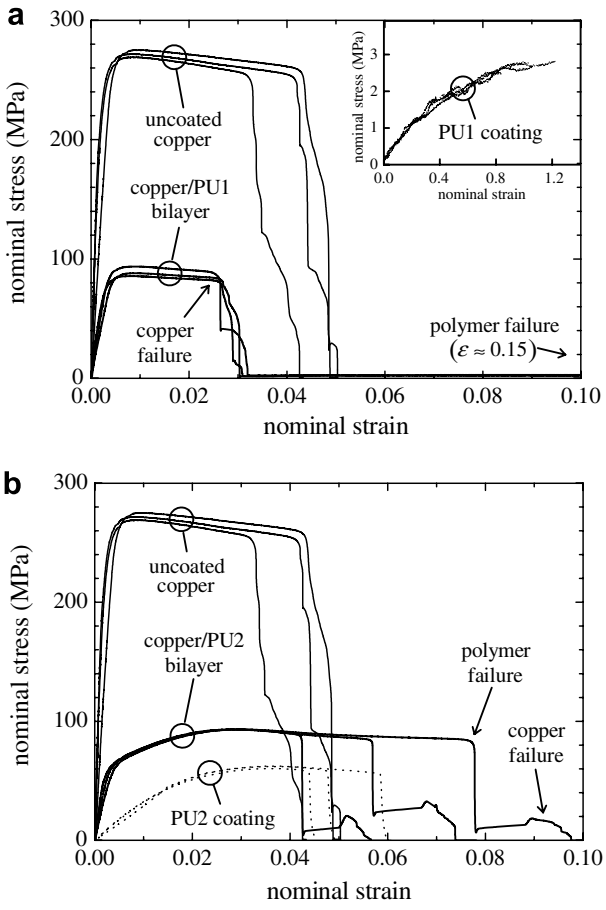

Fig. 3. Quasi-static tensile response (nominal strain rate $\dot{\varepsilon} = 10^{-3}\ s^{-1}$) of uncoated copper (thickness h_m = 0.26 mm), (a) copper/PU1 bilayer (total thickness $h_m + h_p$ = 0.85 mm) and (b) copper/PU2 bilayer (total thickness $h_m + h_p$ = 1.3 mm). The tensile responses of the coating materials alone are also shown. Three specimens of each are presented. The total strain energy dissipated per unit mass, U, is taken as the average of the three specimens.

ings peeled off. The tensile response of the dog-bone shaped polymer specimens were measured in a screw-driven test machine. The tensile strain was estimated using a laser extensometer while the stress was calculated by employing measurements from the load cell of the test machine. The quasi-static (applied nominal strain rate $\dot{\varepsilon} = 10^{-3}\ s^{-1}$) uniaxial tensile responses of PU1 (specimen thickness h_p = 0.68 mm) and PU2 (specimen thickness h_p = 1.29 mm) are included in Fig. 3a and b. Results from three separate tests are included to give an indication of the variability of the results. The tensile response of the PU2 coating is comparable with the compressive response included in Fig. 2b and the reported tensile strength value of 69 MPa (see Table 1). However, the tensile and compressive responses of PU1 are considerably different. Under tension the PU1 coating fails at a nominal stress of approximately 3 MPa corresponding to a nominal tensile strain of 1.2. However, the compressive strength of PU1, as shown in Fig. 2a, is only of the order of 1.4 MPa suggesting that the tensile strength of this material is considerably higher than its compressive peak strength, due to orientation hardening. Moreover, the PU1 tears in tension by a single macroscopic crack while it fragments in compression.

It is worth emphasizing here that both polymers exhibit significant strain rate hardening and do not display a neo-Hookean tensile stress–strain relation (Eq. (2)). Thus, the results presented subsequently cannot be directly compared with the Xue and Hutchinson (2007) predictions.

2.2. Dynamic compressive response of the polymers

The main aim of this study is to investigate the response of copper/polymer bilayers subject to dynamic loading. To ascertain the dynamic stress versus strain characteristics of the two polyurethane coating materials (PU1 and PU2), a series of dynamic compression tests were conducted. The tests were conducted in a screw-driven test machine at intermediate values of strain rate ($\dot{\varepsilon} \approx 1\ s^{-1}$) using test specimens identical to those employed in the quasi-static tests. A Split–Hopkinson bar was used to measure the high strain rate ($10^2\ s^{-1} \leqslant \dot{\varepsilon} \leqslant 10^4\ s^{-1}$) responses: cuboidal PU2 specimens of side 6 mm were tested using Maraging 300 steel bars while the dynamic properties of the PU1 specimens (discs with diameter 5.7 mm and thick-

ness 1.9 mm) were measured using Magnesium bars. The dynamic compressive responses of PU1 and PU2 are included in Fig. 2a and b, respectively. Both polymers display a strong strain rate dependence; for example the compressive yield strength of PU2 rises from 50 MPa under quasi-static conditions ($\dot{\varepsilon} = 1.4 \times 10^{-4}$ s^{-1}) to 150 MPa at an applied compressive strain rate of 1350 s^{-1}. Moreover, the initial modulus of PU1 and PU2 also increase with increasing strain rate (Fig. 2). Following the Xue and Hutchinson (2007) analysis, we anticipate this modulus increase to have a beneficial effect in enhancing the necking strain of the bilayers under dynamic tensile loadings.

3. Quasi-static response of the copper–polymer bilayers

Bilayers comprising copper sheets of thickness h_m = 0.26 mm coated with PU1 or PU2 polymers were tested quasi-statically in order to measure any possible enhancements in energy absorption in line with the predictions of Xue and Hutchinson (2007). Rolled copper sheets of thickness h_m = 0.26 mm and density ρ_m = 9040 kg m^{-3} were coated with a polymer layer using a draw-down bar. Prior to the coating process, the copper sheets were treated with Chemlok 213, a rubber-to-metal adhesive that is manufactured by the Lord Corporation. This adhesive primer ensured an excellent bond between the polymer and the copper with no visible signs of interfacial failure in any of the tests reported here.

3.1. Quasi-static uniaxial tension

The quasi-static tensile response (applied nominal strain rate $\dot{\varepsilon} = 10^{-3}$ s^{-1}) of the uncoated as-received copper (thickness h_m = 0.26 mm) is plotted in Fig. 3. This tensile response was measured using standard tensile dog-bone specimens in a screw-driven test machine in a manner similar to the polymer coatings. The dog-bone specimens had a gauge region of width 12 mm and length 50 mm, and were machined from identical copper sheet of thickness h_m = 0.26 mm as used to produce the bilayer specimens. Three separate measurements are included in Fig. 3 in order to give an indication of the inherent scatter in the material properties of the copper. We observe that the tensile response of the copper is well approximated as an elastic-ideally plastic solid with a tensile yield strength of about 280 MPa and $N \approx 0$ (i.e. ideally plastic response). The maximum applied load is attained at a nominal strain of around 1% but intriguingly necking does not set in immediately after the load maximum. Rather, necking followed by material failure occurs much later at a strain ε_f in the range 4–5%. Some scatter was observed in the measured value of ε_f as indicated in Fig. 3. This delay in necking is not fully understood but is most probably related to the fact that the ratio of the specimen length to width is about four. Numerical calculations by Tvergaard (1993) have shown that necking in these rectangular specimens first occurs in a diffuse mode with the neck on the order to the specimen width. The onset of necking is typically a function of the specimen length to width with necking delayed in shorter specimens.

The measured quasi-static tensile responses of the copper/polymer bilayers coated with PU1 and PU2 are included in Fig. 3a and b, respectively. Here the stress is defined as the *average stress* over the bilayer thickness (i.e. copper plus polymer layers). Note that the strong bond between the copper and the polymer coating meant that the strain in the copper and polymer coatings were approximately equal in these tests. The average coating thicknesses are h_p = 0.59 mm for the bilayer with the PU1 coating and h_p = 1.04 mm for the bilayer with the PU2 coating. In all cases the copper layer has thickness h_m = 0.26 mm. The differences in the coating thicknesses of PU1 and PU2 is a consequence of the draw-down bar application technique. First consider the bilayer with the PU2 coating (Fig. 3b). As the polymer has a much lower yield strength than the copper, the yield strength of the bilayer is significantly below that of the uncoated copper, consistent with a rule of mixtures prediction. However, in line with the Xue and Hutchinson (2007) prediction, the polymer enhances the tensile failure strain of the bilayer with ε_f of the bilayer lying in the range 5–8% compared to failure strains of 4–5% for the uncoated copper. The associated tensile energy absorption capacities per unit mass (averaged over the three tensile tests plotted in Fig. 3b) of the uncoated copper and bilayer specimens are $U_{monolithic}$ = 1.33 kJ kg^{-1} and $U_{bilayer}$ = 1.94 kJ kg^{-1}, respectively (Table 2). Thus, the reduced strength of the PU2 coated bilayer compared to the uncoated copper is offset by the ductility enhancement, giving rise to a 45% higher tensile energy absorption per unit mass. Next consider the bilayer coated with PU1. Again the bilayer has a reduced strength compared to the uncoated copper (Fig. 3a) but also has a slightly reduced ductility compared to the uncoated copper. This small reduction in failure strain is most probably a result of degradation of the copper and polymer as a result of the Chemlok primer coating used to provide the strong bonding between the coating and the copper (note that the polymer fails at a strain $\varepsilon \approx 0.15$ in the bilayer as indicated in Fig. 3a while the polymer on its own has a failure strain in excess of 1.0).[1] Consequently, the energy absorption capacity per unit mass of the copper/PU1 bilayer is approximately half that of the uncoated copper, i.e. $U_{bilayer}$ = 0.76 kJ kg^{-1} for the bilayer with the PU1 coating (Table 2).

Recall that the Xue and Hutchinson (2007) calculations predict that the energy absorption capacity per unit mass of the bilayers increases with increasing coating modulus and thickness. We note that our experimental results are qualitatively consistent with these predictions, i.e. the energy absorption capacity per unit mass of the bilayer with the PU2 coating is considerably higher than the uncoated copper and the bilayer with the PU1 coating. However, we are unable to make quantitative comparisons between the measurements and the predictions as the polymers employed in this study do not obey a neo-Hookean relation as assumed by Xue and Hutchinson (2007). It is worth emphasizing here that the Xue and Hutchinson (2007) predictions suggest that it is necessary to choose a polymer with a sufficiently high stiffness in order to achieve these

[1] The degradation of the copper and coating in the case of the PU2 coating is not sufficient to offset the ductility enhancement due to the stiffer PU2 coating.

Table 2
Measured tensile energy absorption capacities and bulge forming failure pressures of the uncoated copper and PU1 and PU2 bilayers

Material	Tensile energy absorption per unit mass, U (kJ kg^{-1})	Critical bulge forming pressure, p_c (MPa)	Critical bulge forming pressure per unit mass, $\hat{p}_c$ (MPa kg^{-1})
Uncoated copper	1.33	1.36	179
Copper/PU1 bilayer	0.76	1.39	142
Copper/PU2 bilayer	1.94	2.77	266

performance enhancements. Our measurements show that the bilayer with the PU1 coating has a considerably inferior energy absorption capacity on a unit mass basis compared to the uncoated copper: we attribute this to the considerably lower modulus of PU1 compared to PU2.

3.2. Quasi-static bulge forming tests

The Xue and Hutchinson (2007) calculations and the above measurements suggest that appropriately designed metal/polymer bilayers can have a significantly higher energy absorption capacity per unit mass compared to uncoated metallic sheets under uniaxial tension. In most practical applications, such material systems are used in a clamped plate configuration where they are subjected to biaxial stress states. In order to gauge the performance of the coated and uncoated copper plates under biaxial loading, we performed static bulge forming tests on circular plates clamped around their periphery. The performance metric in these tests is taken to be the inflation pressure at the onset of failure in the plates (expressed per unit mass of plate). Three plate configurations were tested:

(i) Uncoated copper plates of thickness $h_m = 0.26$ mm (mass per unit area $m = 2.35$ kg m^{-2}).
(ii) Copper plates of thickness $h_m = 0.26$ mm, coated with a $h_p = 0.56$ mm PU1 layer (mass per unit area $m = 3.04$ kg m^{-2}).
(iii) Copper plates of thickness $h_m = 0.26$ mm, coated with a $h_p = 0.76$ mm PU2 layer (mass per unit area $m = 3.23$ kg m^{-2}).

The polymer coatings were applied as described above using Chemlok 213 primer with the differences in the coating thicknesses between the PU1 and PU2 coatings a consequence of the draw-down bar technique used to apply the coatings.

The bulge forming tests were conducted on circular plates of diameter 102 mm (Fig. 4a) using the apparatus sketched in Fig. 4b. Eight equally spaced clearance holes for M8 bolts were drilled into the copper plates on a pitch circle of radius

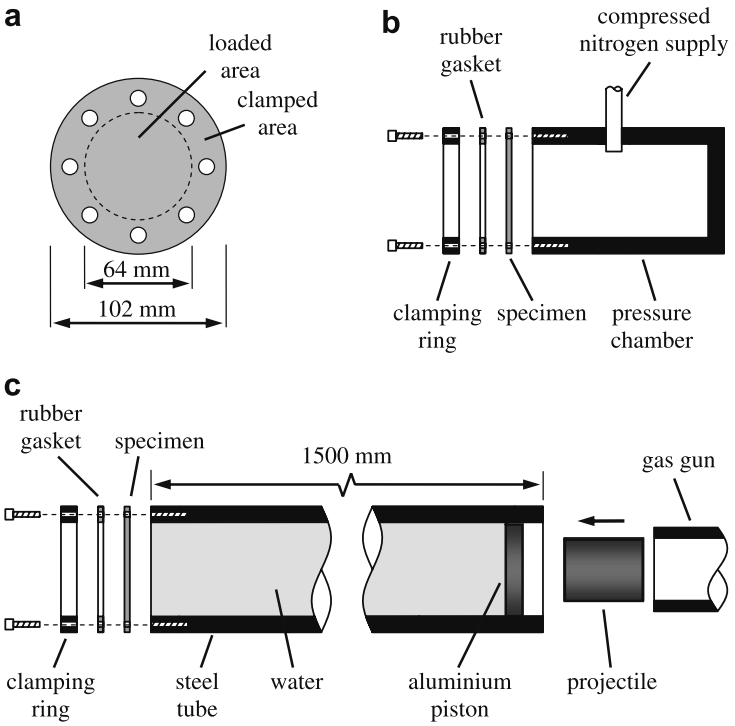

Fig. 4. Outline of the experimental apparatus: (a) the test plate dimensions. (b) Schematic of the static inflation apparatus. (c) Schematic of the water blast apparatus, a water-filled steel tube impacted by a projectile.

Table 3
Analysis of the static bulge forming tests on clamped plates of radius $R = 32$ mm

Material	Critical bulge forming pressure, p_c (MPa)	Specimen thickness, h (mm)	Yield strength, σ_Y (MPa)	Predicted critical strain, $\bar{\varepsilon}_c$
Uncoated copper	1.36	0.26	270	0.0126
Copper/PU1 bilayer	1.39	0.82	87	0.0128
Copper/PU2 bilayer	2.77	1.02	90	0.0331

The predicted critical strains in the plates $\bar{\varepsilon}_c$ at the failure pressures p_c are included in the table along with values of the other parameters required in Eq. (A7).

41 mm, to enable clamping of the copper plate onto the end of a cylindrical pressure vessel of outer diameter 102 mm and inner diameter 64 mm (Fig. 4b). To facilitate this, an annular steel clamping ring was used, of thickness 10 mm, outer diameter 102 mm and inner diameter 64 mm. Thus, the effective radius of the clamped plate, $R = 32$ mm. A 1 mm thick rubber gasket was included between the clamping ring and the specimen in order to provide a uniform contact and ensure a good seal. The clamped test specimen was loaded by gradually increasing the chamber pressure using a high pressure nitrogen gas source. The critical pressure at which the specimen failed was then recorded. The repeatability of the measurements was confirmed by testing three plates of each type (uncoated, PU1 coated and PU2 coated) and the average values of the measured failure pressure are reported below.

The average failure pressure p_c and failure pressure per unit mass $\hat{p}_c$ for the uncoated metal, PU1 coated and PU2 coated plates, respectively, are listed in Table 2. The PU2 coated plates have a significantly higher failure pressure $\hat{p}_c$ while the PU1 coated plates show no performance enhancements over the uncoated plates—this general trend is consistent with the uniaxial tensile results, i.e. that PU2 coated plates have a higher uniaxial tensile energy absorption per unit mass compared to the PU1 coated and uncoated plates (Table 2). This confirms that performance enhancements of bilayers with sufficiently stiff and strong polymer coatings in terms of tensile energy absorption translate to at least some structural loading situations of interest. However, these results do not give us direct information on the ductility enhancements due to the coatings under biaxial stress states.

In order to relate the failure pressure to the corresponding failure strains of the plate material, an approximate analytical model for the quasi-static bulge forming of circular plates made from a rigid-ideally plastic material is presented in Appendix A. The predicted equi-biaxial strains $\bar{\varepsilon}_c$ at the failure pressure are listed in Table 3: the values of the yield strength σ_Y used in these predictions are also listed in Table 3 and follow from Fig. 3. The predicted critical strains in the uncoated copper and PU1 coated plates are both equal ($\bar{\varepsilon}_c \approx 1.2\%$) and approximately equal to the strains at the onset of softening under uniaxial tension (Fig. 3). By contrast, the corresponding critical strains are higher in the PU2 coated plates ($\bar{\varepsilon}_c \approx 3.3\%$) suggesting that the PU2 coating enhances the ductility of the copper even under biaxial stress states.

4. Performance of the copper/polymer bilayers: dynamic bulge forming

Xue and Hutchinson (2007) conducted a numerical investigation into axisymmetric neck development in clamped circular metal/elastomer bilayers subject to impulsive loads. While material failure was not incorporated in their analysis, the calculations suggest that necking is delayed in the clamped circular metal/polymer bilayer plates and thus these plates are able to sustain a higher *spatially uniform* impulse loading compared to uncoated metal plates of the same mass. In this section we report a series of dynamic bulge forming experiments on the bilayer and uncoated copper plates considered in Section 3. The section is organised as follows. First the dynamic bulge forming apparatus, comprising a water shock tube, is described and the relevant non-dimensional groups characterising the loading are identified. Next, the experimental observations and results for both the uncoated and bilayer plates are discussed in light of the relevant non-dimensional loading parameters.

4.1. Underwater shock loading: key non-dimensional groups

Deshpande et al. (2006) have developed an apparatus for the underwater shock loading of materials and test structures within the laboratory. This apparatus, sketched in Fig. 4c, is used to perform the dynamic bulge forming tests on the bilayer specimens. The principle of operation of the shock tube is described in Deshpande et al. (2006) and Kazemahvazi et al. (2007). For the sake of completeness, the essential details are given in Appendix B along with the fluid–structure interaction analysis of Taylor (1941) used to estimate the water shock momentum transmitted to the plate.

Consider clamped circular plates (uncoated or bilayers) of radius R and thickness h made from a rigid-ideally plastic metal of yield strength σ_{Ym} and density ρ_m. The plates are subjected to a spatially uniform underwater blast of the form (A1); an exponentially decaying pressure pulse with peak pressure p_0 and decay constant θ. Following Fleck and Deshpande (2004) we can argue that the response can be temporally decoupled into two stages. First, in a fluid–structure interaction phase, the plate acquires a momentum I_{trans} as given by the Taylor (1941) analysis (see Appendix B for details). Subsequent loading by the water is neglected and the second phase of the response reduces to the classical problem of an impulsively loaded clamped plate as analysed (for small deflections) by Wang and Hopkins (1954). The relevant independent non-dimensional

groups governing the deformation of the plate are (i) the aspect ratio of the plate R/h, (ii) the Taylor fluid–structure interaction parameter ψ and (iii) the non-dimensional transmitted impulse per unit mass $\bar{I}_t \equiv \frac{I_{\text{trans}}}{m}\sqrt{\frac{\rho_m}{\sigma_{Ym}}}$. The dependent non-dimensional groups include the normalised plate displacement w/h and the strain ε in the plate.

In the water shock tube experiments described subsequently, pressure decay constants in the range $\theta = 0.09$–0.15 ms are considered, uncoated copper plates have a mass per unit area $m \approx 2.4$ kg m^{-2} and $m \approx 3.2$ kg m^{-2} for the bilayers, resulting in large values of ψ. In this limit, the Taylor estimate, Eq. (B5), for the transmitted impulse simplifies to

$$I_{\text{trans}} \approx \frac{2p_o m}{\rho_w c_w}, \tag{6}$$

and consequently the non-dimensional transmitted impulse per unit mass

$$\bar{I}_t \equiv \frac{2p_o}{\rho_w c_w}\sqrt{\frac{\rho_m}{\sigma_{Ym}}} \tag{7}$$

is insensitive to the magnitude of θ.

As discussed by Kazemahvazi et al. (2007), the failure modes of the circular plates are insensitive to the value of the plate aspect ratio for $R/h \geqslant 100$ and thus it is sufficient to characterise the failure modes of the uncoated and bilayer plates in terms of (i) the non-dimensional transmitted impulse per unit mass $\bar{I}_t$ and (ii) the non-dimensional mass of the plates $\overline{M} \equiv 1/\psi$ which is interpreted as the ratio of the mass of the plate to the mass of the water contained within the blast pulse (per unit area). In the experiments described subsequently the thickness of the copper layer $h_m = 0.26$ mm is held fixed and thus the coated and uncoated specimens have different masses. In order to make a fair comparison we shall keep the independent non-dimensional group $\overline{M}$ fixed and increment the value of $\bar{I}_t$ to investigate the deformation and failure modes. The value of the non-dimensional impulse per unit mass at the onset of failure is used as the key performance metric to investigate possible enhancements in the blast mitigation capabilities of the bilayer plates over the uncoated plates.

4.2. Specimen configuration and test protocol

Clamped circular uncoated copper plates and copper/polymer bilayer plates of diameter 102 mm were tested using the water shock tube sketched in Fig. 4c. The specimen and clamping configuration were identical to those employed in the static bulge forming tests. The water column is located in a steel tube of length $L = 1.5$ m, internal diameter $\phi = 64$ mm and wall thickness $w = 19$ mm. The tube is capped at one end by a 10 mm thick aluminium piston and at the opposite end by the copper specimen. The piston has an O-ring seal and contains a bleed valve to ensure that air is not trapped in the water column as detailed by Deshpande et al. (2006). Dynamic loading is achieved by firing steel circular cylinders of diameter $d = 50$ mm and mass in the range 0.3–0.6 kg at the piston. The projectiles are accelerated using a gas gun of barrel length 4.5 m and inner diameter $d = 50$ mm. No sabot is employed and the bursting of copper shim diaphragms forms the breach mechanism of the gas gun. The projectile velocity ranges from 15 ms^{-1} to 85 ms^{-1} and is measured at the exit of the barrel using laser-velocity gates. The pressure transient in the water tube was measured using a hoop strain gauge placed 200 mm from the impacted end of the water shock tube.

As discussed in Appendix B, the peak pressure p_0 and the decay time θ of the pressure transients in the shock tube were controlled by varying the projectile velocity and mass, respectively. The decay time θ was varied with m in order to keep $\overline{M}$ fixed, while $\bar{I}_t$ was controlled by the choice of p_0. High speed photographic sequences of the dry face of the plates were taken using a DRS Technologies Ultra 8 camera, thereby allowing for direct observation of the sequence of deformation and failure modes of the plates. A select number of repeat tests were conducted for each specimen type and $\overline{M}$ value in order to confirm the repeatability of the test results in terms of the failure modes.

4.3. Summary of results: uncoated plates

Results are described for the $H_m = 0.26$ mm copper plates subjected to water shocks with decay constants $\theta = 0.12$ ms ($\overline{M} = 0.014$) and $\theta = 0.087$ ms ($\overline{M} = 0.020$) and peak pressures in the range $p_0 = 25$–56 MPa, see Table 4. Post-test photographs of the copper plates subject to shocks with a decay constant $\theta = 0.12$ ms ($\overline{M} = 0.014$) are shown in Fig. 5. The deformation and failure modes are sub-divided into four modes consistent with those observed by Kazemahvazi et al. (2007) for uncoated copper plates subjected to an underwater blast. An outline of these failure modes is given here, but a detailed description of the progress of deformation and failure and the associated timescales may be found in Kazemahvazi et al. (2007).

(i) *No failure (Fig. 5a).* At low blast pressures ($p_0 < 33$ MPa), the plate undergoes plastic bending and stretching but no failure is observed (Fig. 5a). Consistent with the observations of Kazemahvazi et al. (2007), high speed photography revealed that the deformation mode involves plastic hinges travelling from the periphery to the centre of the plate, followed by stretching and bending of the plate in a manner similar to the quasi-static deformation mode of a clamped circular plate under uniform transverse pressure. This deformation history supports several theoretical predictions (e.g. Wang and Hopkins, 1954; Florence, 1966).

Table 4
Experimental parameters for the coated and uncoated plates subject to uniform and localised water blast loading

Specimen type	Average mass (kg m^{-2})	Average coating thickness (mm)	θ (ms)	p_0 (MPa)	$\overline{M}$	$\overline{I}_t$
(a) Uniform loading						
Uncoated	2.37	–	0.122	25.0–81.5	0.014	0.20–0.66
Uncoated	2.38	–	0.087	32.8–58.3	0.020	0.26–0.47
PU2 coated, weak bond	3.47	0.76	0.122	24.0–52.7	0.021	0.19–0.43
PU2 coated, strong bond	3.55	0.98	0.122	25.1–45.6	0.021	0.20–0.37
PU1 coated, weak bond	3.36	0.77	0.122	23.2–51.4	0.019	0.19–0.41
PU1 coated, strong bond	3.02	0.58	0.095	24.9–48.6	0.023	0.20–0.39
(b) Localised loading						
Uncoated	2.39	–	0.122	30.0–82.2	0.014	0.24–0.66
PU2 coated, weak bond	3.03	0.42	0.152	22.8–34.7	0.014	0.18–0.28
Uncoated	2.35	–	0.087	36.8–91.5	0.019	0.30–0.74
PU2 coated, weak bond	3.23	0.62	0.122	25.3–40.3	0.019	0.20–0.33

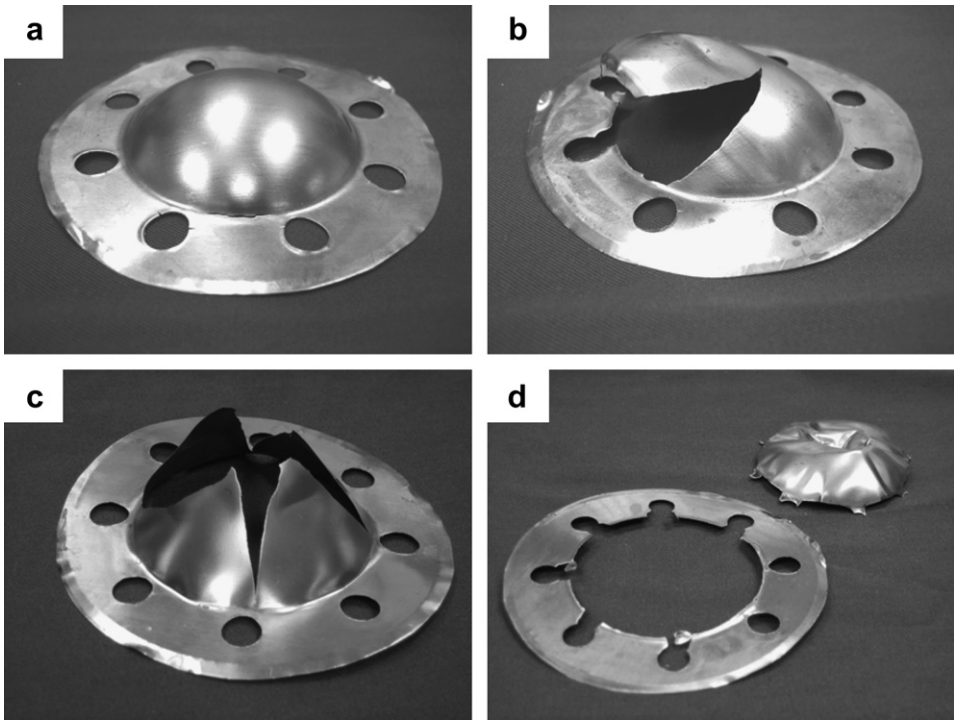

Fig. 5. Deformation modes of uncoated copper plates, $\overline{M} = 0.014$: (a) no failure ($\overline{I}_t = 0.24$, $p_0 = 30$ MPa), (b) intermediate failure ($\overline{I}_t = 0.28$, $p_0 = 35$ MPa), (c) petalling failure ($\overline{I}_t = 0.34$, $p_0 = 42$ MPa) and (d) complete failure at the supports ($\overline{I}_t = 0.45$, $p_0 = 56$ MPa).

(ii) *Intermediate failure (Fig. 5b).* For blast pressures in the range 33 MPa $\leqslant p_0 \leqslant$ 40 MPa, failure initiates near the supports by tearing around the clamping bolts. This failure mode is expected to be sensitive to the clamping conditions, and it is anticipated that it would not be present in the case of ideally clamped plates where all relative motion of the portion of the plate between the clamping ring and the water tube was prevented.

(iii) *Petalling failure (Fig. 5c).* Petalling failure of the plates is observed for peak pressures over the range 40 MPa $\leqslant p_0 \leqslant$ 49 MPa. Petalling failure initiates at the plate centre after the coalescence there of plastic hinges travelling from the periphery. Subsequently, cracks propagate radially outwards towards the clamped boundary (see Kazemahvazi et al. (2007) for high speed photographs of this failure sequence).

(iv) *Tearing at the supports (Fig. 5d).* At high blast pressures ($p_0 >$ 49 MPa), complete failure occurs at the supports prior to the development of petalling. The current investigation focuses on the onset of failure; an in-depth investigation of the entire range of failure modes of plates subject to a water blast is given in the parallel study of Kazemahvazi et al. (2007).

The observed deformation and failure modes of the uncoated copper plates subject to water blasts with decay constants $\theta = 0.12$ ms ($\overline{M} = 0.014$) and $\theta = 0.087$ ms ($\overline{M} = 0.020$) are summarised in Fig. 6. The blast intensities are plotted in terms of

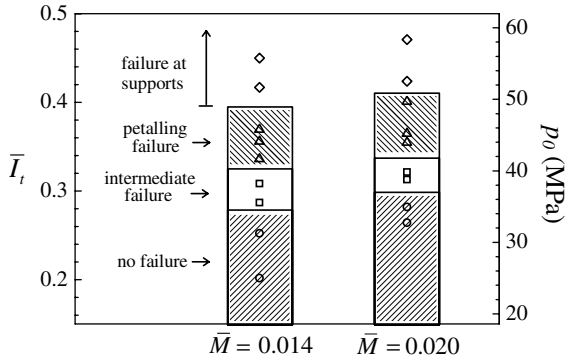

Fig. 6. Failure modes of clamped uncoated copper plates subjected to uniform blast loading. Results are shown for two values of non-dimensional plate mass $\bar{M}$. The symbols denote an experimental data-point in the regime indicated.

the non-dimensional transmitted impulse per unit mass $\bar{I}_t$ corresponding to peak blast pressures in the range $p_0 = 25$–60 MPa. The boundaries between the failure modes (in terms of $\bar{I}_t$) are reasonably insensitive to the value of $\bar{M}$.

4.4. Summary of results: copper–polyurethane bilayer plates

The deformation and failure modes of the uncoated copper plates are now compared with identical plates coated with the two types of polyurethane: PU1 and PU2. The polymer coatings are applied to copper plates of thickness $h_m = 0.26$ mm using a draw-down bar technique, as described in Section 3. The PU1 bilayers had an average coating thickness $h_p \approx 0.66$ mm while $h_p \approx 0.84$ mm for the PU2 bilayers. Some variability in the coating thicknesses results from the drawn-down bar application technique. For each condition listed in Table 4, the coating thicknesses of the test specimens fall within a range of ±0.25 mm of the average value. To ascertain the effect of bond strength between the polymer and the metal, two methods of applying the polymer coating were considered:

(i) *Weak adhesion.* Here the polymer is applied directly onto the copper plate with no priming or pre-treatment.
(ii) *Strong adhesion.* Prior to coating, a primer coat of Chemlok 213 adhesive is applied. This results in an excellent bond between the polymer coat and the copper plate. No interfacial delamination is observed in any of the tests reported subsequently when this method of applying the polymer coat was employed.

The circular test specimens were clamped to the steel tube with the copper side facing the blast (the wet side) and the polymer on the dry side. The rubber gasket and clamping ring were fastened in contact with the polymer coating, as sketched in Fig. 4c. In all tests, the non-dimensional mass of the plates was fixed at $\bar{M} = 0.020$ to allow for a direct comparison with the uncoated plate results of Section 4.3. This was achieved by choosing an appropriate value for the blast decay constant θ in line with the areal mass m of the bilayer plates; see Table 4. The variability of the coating thicknesses (and therefore plate masses) results in $\bar{M}$ falling within the range 0.019–0.023 for the experimental specimens included in Table 4. With $\bar{M}$ fixed, the failure modes of the plates were investigated by gradually increasing $\bar{I}_t$ via the peak pressure p_0. A detailed study of the effect of $\bar{M}$ and the associated fluid–structure interaction effect in the metal/polymer bilayers is beyond the scope of this work.

The observed deformation and failure modes for the uncoated copper plates subject to water blasts with decay constant $\theta = 0.087$ ms ($\bar{M} = 0.020$) are compared with PU1 and PU2 coated bilayer plates in Fig. 7a and b, respectively. Over the range of blast pressures considered here the four failure modes identified for the uncoated plates persist in the bilayers. We proceed to discuss these observations in some detail. First consider the PU2 coated plates. The boundaries between the failure modes occur at approximately the same values of $\bar{I}_t$ (or p_0) for the uncoated plates and for the PU2 bilayer plates with a weak bond between the polymer and metal. By contrast, the PU2 bilayer plates with a strong bond between the polymer and metal fail at significantly smaller values of $\bar{I}_t$. Photographs of the deformed/failed uncoated and bilayer plates for selected values of $\bar{I}_t$ are included in Fig. 8. These photographs clearly show that the bilayer plates with the strongly bonded polymer coatings are significantly more prone to failure for a given $\bar{I}_t$ (or p_0) compared to the uncoated copper plates or bilayer plates with weakly bonded polymer coatings. These findings can be rationalised as follows:

(i) *Weakly bonded PU2 coatings* do not provide any significant performance enhancements for plates subject to water shock loading. This can be understood by examining the sequence of high speed photographs shown in Fig. 9a for a weakly bonded PU2 bilayer plate subject to a blast with peak pressure $p_0 = 46$ MPa ($\bar{I}_t = 0.37$). The images show the polymer coated side of the plate (the dry side) during petalling failure. Under these dynamic loading conditions, the polymer fractures early in the deformation history. It is noted from Fig. 9b that in the third frame, by which time

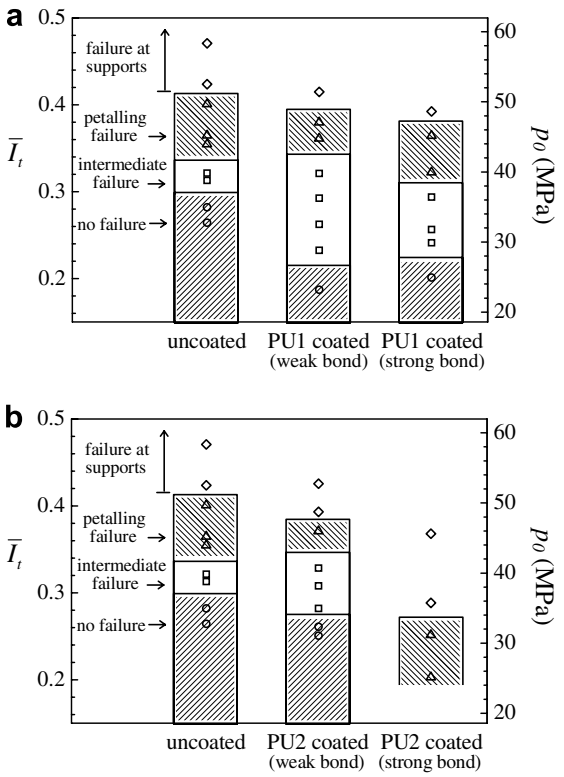

Fig. 7. Failure modes of clamped bilayer plates subjected to uniform blast loading: (a) PU1 coated, (b) PU2 coated. Results shown are for $\overline{M} = 0.020$. The symbols denote an experimental data-point in the regime indicated.

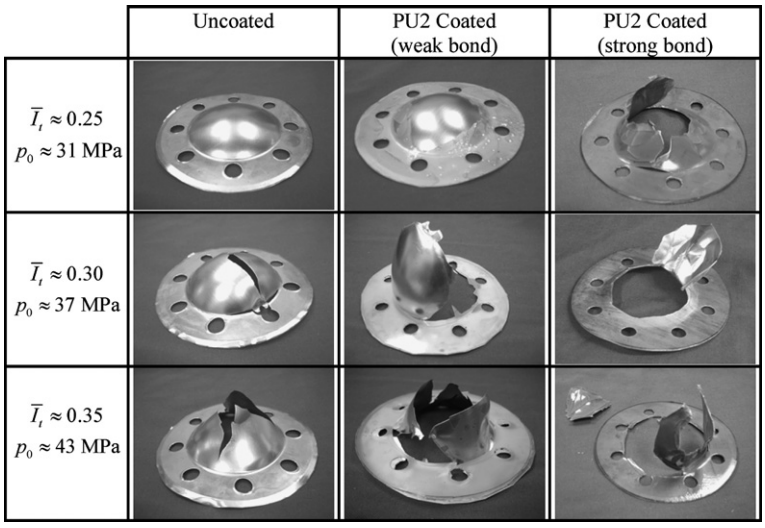

Fig. 8. Comparison of final plate shapes for uniformly loaded uncoated copper, PU2 coated with weak adhesion and PU2 coated with strong adhesion. Results shown are for $\overline{M} = 0.020$.

the plastic hinges have reached the centre of the plate, the coating has entirely detached, exposing the copper substrate. This fracturing and subsequent spalling of the coating (due to the weak adhesion with the underlying metal) eliminates its capability to provide any ductility enhancement compared to the uncoated plate. The ability of the PU2 coating to retard neck formation, as observed quasi-statically (Section 3, above), is thus not realised under dynamic bulge forming conditions.

(ii) More surprisingly, the performance of the bilayer plates with PU2 *strongly bonded* to the copper plates is inferior to the uncoated plates. A high speed photographic sequence of the response of a strongly bonded PU2 bilayer subjected to a blast with peak pressure $p_0 = 25$ MPa ($\bar{I}_t = 0.20$) is included in Fig. 9b. Again, the images show the polymer coated side of the plate (the dry side) during petalling failure. We observe that the coatings fracture but, in contrast to Fig. 9a, stay adhered to the copper plates. Photographs of the failed weakly and strongly bonded PU2 bilayers are shown in Fig. 10. The coating delamination in the weakly bonded case is evident (Fig. 10a). By contrast, no delamination is evident in the strongly bonded case as seen from the photographs of the dry side (Fig. 10b). In fact the fracture pattern in the polymer, which remains adhered to the substrate, appears duplicated in the copper as seen from the wet side photograph (Fig. 10c). The poor performance of these plates is due to the following factors:

(a) The strongly bonded coating loses ductility at high strain rates and cracks early during the dynamic deformation of the bilayers (Fig. 9b) and thus adds mass without providing any enhancement in energy absorbing capacity.
(b) The fact that the fracture pattern in the polymer is duplicated in the copper (Fig. 10c) indicates that polymer failure occurs while there is still a substantial water pressure loading applied on the plate. The copper is forced into the gaps in the cracked coating, introducing large imperfections and contributing to premature failure of the plate.
(c) Stress concentrations develop in the copper plate immediately adjacent to the cracks in the polymer, resulting in tensile necks initiating in the copper plate.

Next consider the copper plates with the lower modulus PU1 coating. PU1 is above its glass transition at room temperature, and therefore more ductile than PU2. The quasi-static tensile stretching and the static bulge forming measurements reported above indicate that the low modulus PU1 coating provides no performance enhancements under static loading conditions. The summary of measurements of the PU1 bilayers (Fig. 7a) indicate that the coating also does not have any appreciable effect on the failure modes of the copper plates under dynamic loading: the failure modes for a given value of $\bar{I}_t$ are similar for the uncoated copper plates and the bilayer plates with the weak and strongly adhered PU1 coatings. There is a slight reduction in the value of $\bar{I}_t$ at the onset of petalling failure for the strongly bonded PU1 coating. As noted previously for the quasi-static uniaxial tensile tests, this may be an effect of the Chemlok primer coating. This is further exemplified in Fig. 11 where photographs of the as-tested uncoated and PU1 coated plates are included for selected values of $\bar{I}_t$.

4.5. Retrofitting polymer coatings to existing structures

Above, we have compared the performances of the uncoated and coated plates in terms of the transmitted momentum per unit mass $\bar{I}_t$. Another problem of practical interest might involve retrofitting existing structures in order to enhance their dynamic rupture performance. We now consider the potential for the polyurethane coatings to fulfil this role as these coatings are relatively easy to apply to existing structures.

The problem here is therefore to compare the dynamic performance of the uncoated plate with that of the same plate with the polyurethane coating. Thus, the two structures do not have equal mass and it would be appropriate to compare the performances of the coated and uncoated plates in terms of the total impulse I_0 rather than the transmitted impulse per unit mass. To facilitate this comparison we define a non-dimensional total incident impulse

$$\bar{I}_0 \equiv \frac{I_0}{R\sqrt{\rho_m \sigma_{Ym}}}. \tag{8}$$

We re-plot the PU2 bilayer data in Fig. 7b in terms of $\bar{I}_0$ in Fig. 12. It is clear from Fig. 12 that in terms of total incident impulse $\bar{I}_0$, the bilayer with the weakly bonded coating now *outperforms* the uncoated plates. This is rationalised by noting that whilst the added mass of the coating increases the transmitted impulse slightly, the heavier structure acquires a lower kinetic energy and hence had to stretch less in order to dissipate the kinetic energy it has acquired from the incoming water shock. It is worth clarifying here that we avoid a comparison between the uncoated and the PU1 coated plates as the mass of the PU1 coatings has a larger variability (see Table 4) making a comparison between the uncoated and coated plates more difficult to interpret.

4.6. Clamped plates subject to localised dynamic loading

Xue and Hutchinson (2007) show an increased effectiveness of the bilayer configuration in the case of a clamped circular plate with impulsive loading concentrated over a central patch. The experimental results described in Section 4 all pertained to uniform loading of the uncoated and bilayer plates. We now proceed to investigate the performance of clamped plates of diameter 64 mm subject to a water blast load over a localised central patch of diameter 21 mm. Uncoated and bilayer plates with a weakly bonded PU2 coating are considered for two values of the non-dimensional plate mass $\overline{M} = 0.014$ and 0.020.

The experiments were conducted using the water tube apparatus described in Section 4 with the plates clamped to the water shock tube as sketched in Fig. 4c. To achieve the localised central loading a 10-mm thick annular steel ring of diameter 102 mm with a central hole of diameter 21 mm was placed at one end of the water shock tube in contact with the test plate. This additional annular ring is sufficiently thick so as to not deform when subject to the blast pressures employed here: the ring shields the outer rim of the test plate from the water shock. As discussed by Qiu et al. (2005), the deformation of impul-

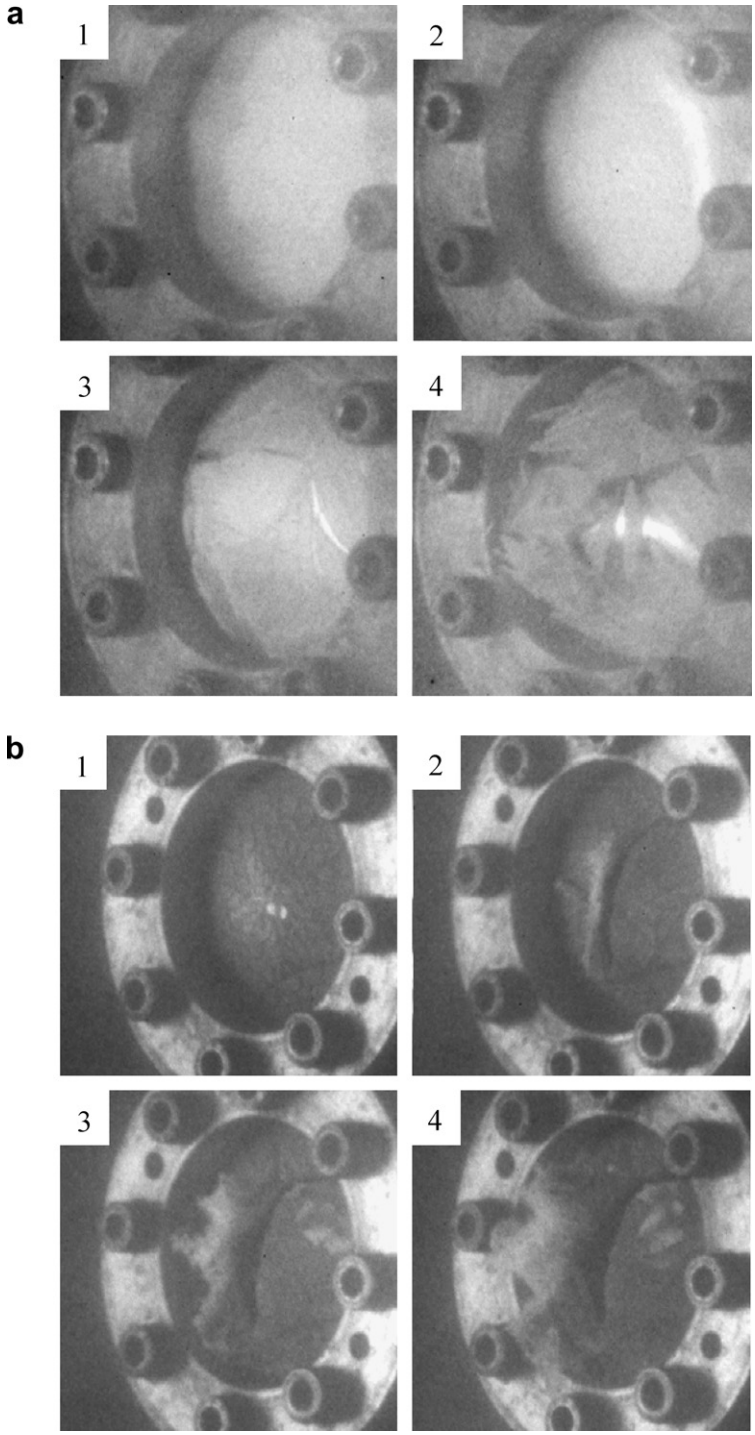

Fig. 9. High speed photography capturing the petalling failure mode in (a) copper with weakly adhered PU2 ($\overline{M} = 0.022$, $\bar{I}_t = 0.37$, $p_0 = 46$ MPa, 180 μs inter-frame time) and (b) copper with strongly adhered PU2 ($\overline{M} = 0.020$, $\bar{I}_t = 0.20$, $p_0 = 25$ MPa, 180 μs inter-frame time).

sively loaded plates loaded over a central patch involves the propagation of hinges from the periphery of the loading patch towards the clamped supports. These travelling hinges were observed in the high speed photographs (not included for the sake of brevity) of the experiments, thus confirming the localised nature of the loading.

Unlike the uniformly loaded case, only two deformation modes are observed for patch loading of the uncoated copper plates over a similar range of peak blast pressures p_0 (or $\bar{I}_t$ values): (i) no failure and (ii) petalling failure. The observed deformation and failure modes for the uncoated copper plates and bilayers with a weakly bonded PU2 layer are summarised in

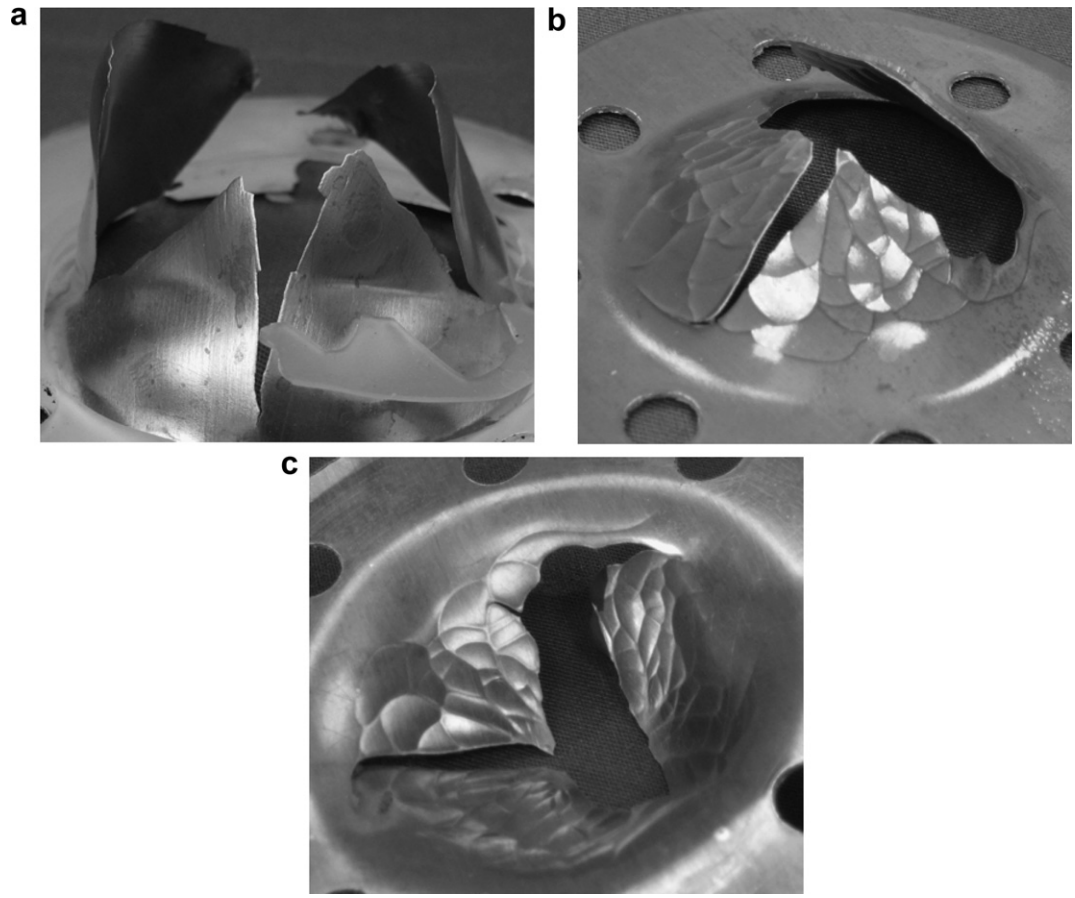

Fig. 10. Details illustrating the final shape for PU2 coated specimens showing petalling failure ($\overline{M} = 0.020$): (a) weakly bonded PU2 ($\bar{I}_t = 0.37$, $p_0 = 46$ MPa); (b) strongly bonded PU2 (dry side view, $\bar{I}_t = 0.20$, $p_0 = 25$ MPa); (c) strongly bonded PU2 (wet side view).

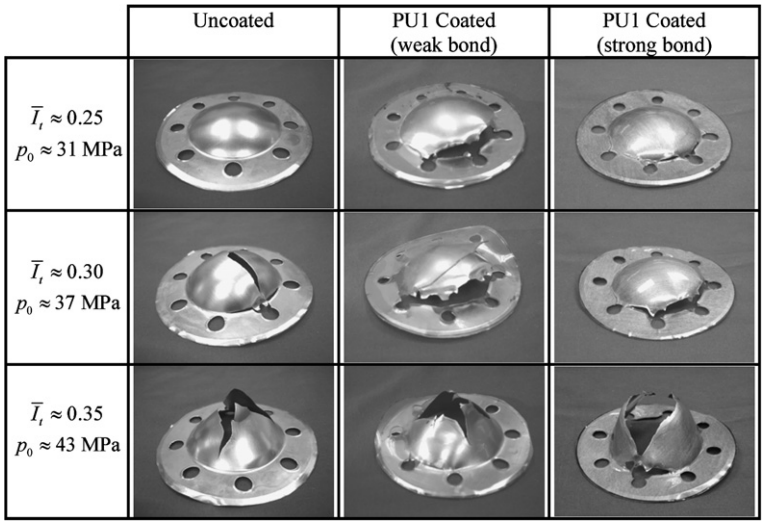

Fig. 11. Comparison of final plate shapes for uniformly loaded uncoated copper, PU1 coated with weak adhesion and PU1 coated with strong adhesion. Results shown are for $\overline{M} = 0.020$.

Fig. 13 for the choices $\overline{M} = 0.014$ and 0.020. Again, the failure modes are reasonably insensitive to the value of $\overline{M}$ over the range considered here. However, in marked contrast to the uniformly loaded cases, failure occurs at about a 25% higher value

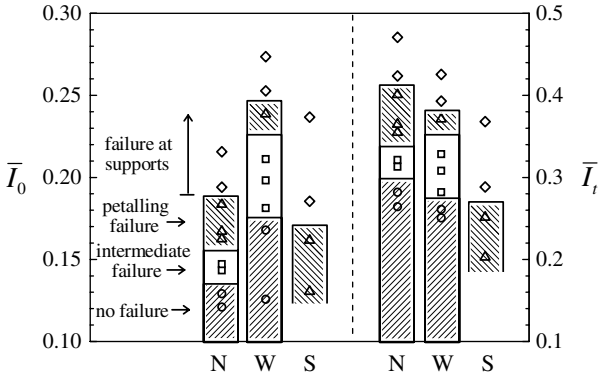

Fig. 12. Failure modes of clamped PU2 coated copper plates subjected to uniform blast loading using two measures of blast loading: $\bar{I}_0$ and $\bar{I}_t$. N, no coating; W, weakly bonded coating; and S, strongly bonded coating. Results shown are for $\overline{M} = 0.020$. The symbols denote an experimental data-point in the regime indicated.

of $\bar{I}_t$ in uncoated plates compared to PU2 coated plates. This is also clearly seen in the photographs of the tested plates included in Fig. 14 for two selected values of $\bar{I}_t$: while petalling failure is observed for the coated plate at $\bar{I}_t \approx 0.28$, the uncoated plate shows no visible signs of failure.

It is worth emphasizing that these experimental results are contrary to the predictions of Xue and Hutchinson (2007) which suggested that polymer coated metallic plates would have significant performance benefits over uncoated plates under localised dynamic loading situations. A possible explanation for this discrepancy is as follows. Localised loadings typically result in much higher strains in the plates (especially near the periphery of the loading patch) than that experienced by plates subjected to spatially uniform blast loadings; compare the dish-like deformed shape of the plate in Fig. 5a with the more conical shape in Fig. 14. Under dynamic loadings, PU2 fractures at relatively small strains and thus adds mass while providing no reinforcement. This premature dynamic failure of the polymer was not accounted for in the Xue and Hutchinson (2007) study and hence their predictions are contrary to the observations made here.

5. Concluding remarks

The role of polymeric coatings in enhancing the underwater blast performance of thin copper plates has been investigated experimentally using a laboratory water shock tube. Two polyurethane polymer coatings were considered in this study: (i) PU1 with a glass transition temperature $T_g = -56$ °C, and (ii) PU2 with $T_g = 49$ °C. Thus, at room temperature PU1 and PU2 are above and below their respective glass transition temperatures and thus offer coatings with a significant contrast in stiffness and ductility. All the copper/polymer bilayers investigated here had a polymer coating of thickness approximately twice that of the metal layer.

Under quasi-static tensile loading, the bilayers with PU2 coatings exhibit a 45% higher energy absorption capacity per unit mass compared to the uncoated copper plates. However, the energy absorption capacity per unit mass of the bilayers with the lower stiffness PU1 coating is approximately half that of the uncoated copper plates. Similarly, the PU2 coating also enhances the static bulge forming failure pressure and strains of clamped circular copper plates. These findings support the arguments of Xue and Hutchinson (2007) that an adequately stiff polymer is required to achieve a synergistic effect between

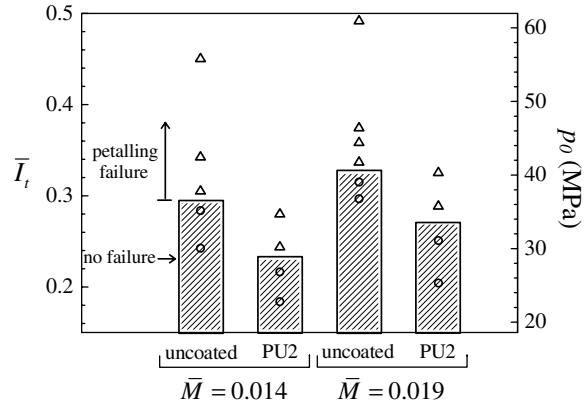

Fig. 13. Failure modes of clamped coated copper plates subjected to localised blast loading, comparing uncoated plates with plates coated with weakly bonded PU2. The symbols denote an experimental data-point in the regime indicated.

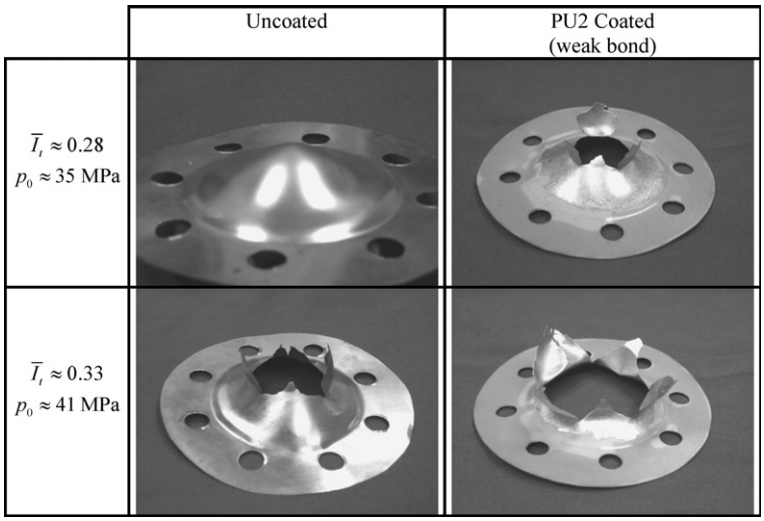

Fig. 14. Comparison of final plate shapes for patch loaded uncoated copper and PU2 coated with weak adhesion. Results shown are for $\overline{M} = 0.019$.

the metal and polymer layers. However, the polymer coatings investigated here do not display a neo-Hookean tensile stress–strain relation and thus the experimental results of this study cannot be directly compared with the Xue and Hutchinson (2007) analysis.

Two types of underwater shock loading tests were performed in this study with peak pressures in the range $p_0 = 25$–60 MPa: (i) spatially uniform loading of the plates and (ii) loading of the plates over a localised central patch, both with the polymer on the dry side of the plates. While petalling and failure at the supports were the observed failure modes under spatially uniform dynamic loading, the patch loaded plates only failed by a petalling mode over the whole range of blast pressures considered here. On an equal mass basis, the performance of the PU2 bilayers with a weakly bonded polymer coating was comparable to the uncoated plates: the low dynamic ductility of PU2 and spalling of the coating negates the performance enhancement observed under quasi-static conditions. Intriguingly, when PU2 was strongly adhered to the copper plates the performance of these bilayers was inferior to the uncoated plates due to cracking of the adhered coating very early in the deformation history of the plates. Stress concentrations develop in the copper plate in the vicinity of the cracks in the polymer, resulting in premature failure of the plates. Consistent with the quasi-static results, the bilayers with the PU1 coatings always underperformed compared to uncoated plates of equal mass. Under localised loading conditions, the low dynamic ductility of the coatings results in the uncoated plates having a superior performance to the bilayers.

In summary, while the PU2 polyurethane coating does provide performance enhancements under quasi-static loading, none of the coatings tested here provide any significant enhancements to the blast mitigation potential of metallic plates when the results are viewed on an equal mass basis. The inferior dynamic performance of the coatings is primarily attributed to their low dynamic ductility. However, the results suggest that for a given total blast impulse, adding mass to the structure in the form of a polyurethane coating may provide a benefit in performance. A comparison with other strategies for adding mass is, however, beyond the scope of this work.

This experimental study has highlighted that polymers with both a high modulus and strength and a high dynamic tensile ductility are required to enhance blast mitigation benefits for polymer/metal bilayers. The mechanical properties of polyurethane and related polyurea based polymers are highly tailorable by manipulation of their molecular structure. The exploration of polymers with higher modulus, strength and ductility and the investigation of the performance of bilayers made from these engineered polymers will form the basis of future studies.

Acknowledgments

This work has been performed as part of the *Ultralight Metallic Panels with Textile Cores Designed for Blast Mitigation and Load Retention* program conducted by a consortium of Universities consisting of Harvard University, Cambridge University, the University of California at Santa Barbara and the University of Virginia. The Office of Naval Research (ONR), monitored by Dr. David Shifler, funded the consortium's work under Grant No. N00014-01-1-1051.

Appendix A. Analysis of the static bulge forming experiment

Consider a clamped circular plate of radius R and thickness h made from a rigid-ideally plastic material with a yield strength σ_Y. For mid-point deflections δ of the plate large compared to h, the plate assumes the shape of a spherical cap with a radius of curvature a as sketched in Fig. A1. Geometry dictates that a, R and δ are related by

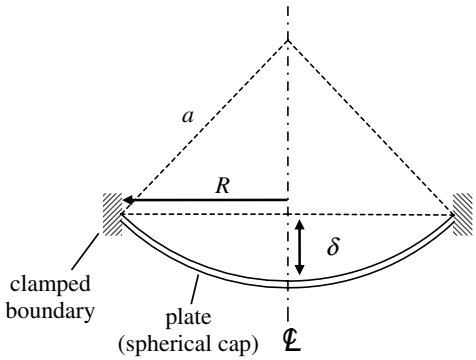

Fig. A1. Sketch of the assumed deformed profile of the clamped plate in the static bulge forming tests. The relevant geometrical parameters are labelled: the plate radius $R = 32$ mm, the mid-point deflection δ and the radius of curvature of the spherical cap a.

$$a = \frac{R^2 + \delta^2}{2\delta}, \tag{A1}$$

with the surface area of the cap and volume swept through by the cap given by

$$A \equiv 2\pi a\delta \tag{A2}$$

and

$$V = \frac{1}{6}\pi\delta\left(3R^2 + \delta^2\right), \tag{A3}$$

respectively. The surface area of the plate has increased from πR^2 to A due to in-plane straining of the plate. Assuming uniform in-plane straining, the radial and circumferential strains at any location within the plate follow as

$$\bar{\varepsilon} \equiv \varepsilon_{rr} = \varepsilon_{\theta\theta} = \frac{1}{2}\left(\frac{\delta}{R}\right)^2, \tag{A4}$$

while the von Mises yield criterion dictates that the in-plane radial and circumferential stresses at yield are given by $\sigma_{rr} = \sigma_{\theta\theta} = \sigma_Y$. Thus, an incremental work balance relation in terms of the applied pressure p reads as

$$p\mathrm{d}V = (\sigma_{rr}\mathrm{d}\varepsilon_{rr} + \sigma_{\theta\theta}\mathrm{d}\varepsilon_{\theta\theta})\pi R^2 h = 2\sigma_Y \pi R^2 h \mathrm{d}\bar{\varepsilon}. \tag{A5}$$

Substituting from (A3) and (A4) gives the pressure in terms of the strain $\bar{\varepsilon}$ in the plate as

$$p = 12\sigma_Y\left(\frac{h}{R}\right)\frac{\sqrt{2\bar{\varepsilon}}}{3 + 6\bar{\varepsilon}}. \tag{A6}$$

Thus, the strain $\bar{\varepsilon}_c$ at the critical pressure p_c is given by

$$\bar{\varepsilon}_c = \frac{1 - 18\bar{p}_c^2 - \sqrt{1 - 36\bar{p}_c^2}}{36\bar{p}_c^2}, \tag{A7}$$

where the normalised critical pressure $\bar{p}_c$ is defined as

$$\bar{p}_c \equiv \frac{p_c R}{12 h \sigma_Y}. \tag{A8}$$

Appendix B. Theory of the water shock tube and the Taylor fluid–structure interaction analysis

The principle of operation of the water shock apparatus and the Taylor fluid structure interaction analysis is briefly summarised in this Appendix. A water column, contained within a thick-walled steel tube, is capped at one end by the test structure and by a piston at the other end. The piston is struck by a steel projectile, as sketched in Fig. 4c, generating a pressure pulse that decays exponentially with time in the water. Similar to realistic underwater blasts, the pulses have the form

$$p = p_0 \mathrm{e}^{-t/\theta}, \tag{B1}$$

where p_0 is the peak pressure and θ is the decay constant. The apparatus is capable of generating peak pressures in the range 10–300 MPa with decay times ranging from 0.05 ms to 1.5 ms. The peak pressure and the decay time are adjusted independently by varying the projectile velocity and mass, respectively. In particular, using one-dimensional linear wave theory, Deshpande et al. (2006) have shown that (p_0, θ) are related to the combined projectile and piston mass per unit shock tube area and initial velocity v_p by

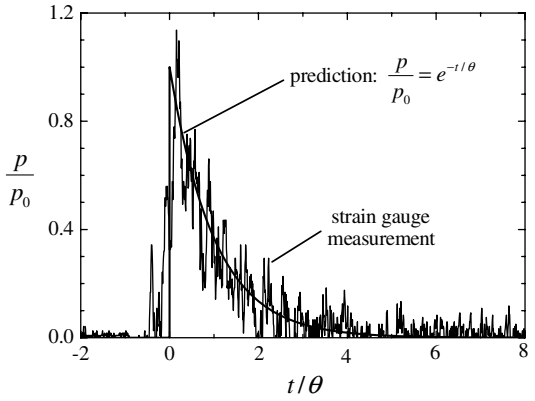

Fig. B1. An example of the generated blast pulse in the water as measured using a strain gauge on the outer wall of the steel tube for $p_0 = 53$ MPa, $\theta = 0.12$ ms.

$$p_0 = \rho_w c_w v_p \tag{B2a}$$

and

$$\theta = \frac{m_p}{\rho_w c_w}, \tag{B2b}$$

where ρ_w is the density of water and c_w is the speed of sound in water. To verify the predictions for peak pressure and decay constant, we measured the pressure in the water using a strain gauge mounted on the exterior surface of the steel tube 200 mm from the impacted end. Fig. B1 shows a comparison between the measured and predicted pressure pulses for a case with $v_p = 37.6\ \mathrm{ms}^{-1}$ and $m_p = 171\ \mathrm{kg\,m}^{-2}$. In Fig. B1, the pressure p and time t are normalised by the predicted values of $p_0 = 53$ MPa and $\theta = 0.12$ ms with $t = 0$ corresponding to the time of arrival of the pulse at the measurement location. Good agreement is achieved over a wide range of blast intensities, and thus in this study the reported values of p_0 and θ are those predicted by Eq. (B2).

This water shock tube is used in this study to load plates of mass per unit area m. The momentum transmitted to the plate can be estimated using the one-dimensional fluid–structure interaction analysis of Taylor (1941) for an underwater pressure pulse of the form (B1) impinging on a free standing plate. When this pressure wave hits a stationary rigid plate at normal incidence, it imparts an impulse

$$I_0 = 2\int_0^\infty p_0 e^{-t/\theta} dt = 2p_0\theta, \tag{B3}$$

to the plate. The factor of two arises in relation (B3) due to full reflection of the pressure wave. If instead, the pressure wave impacts a free standing plate of mass per unit area m, the imparted impulse is less than I_0, and can be estimated as follows. When the pressure wave strikes a free standing plate, it sets the plate in motion and is partly reflected. Cavitation of the water occurs when the pressure at the interface between the plate and the fluid drops to zero; this occurs at a time τ_c after initial impingement given by

$$\frac{\tau_c}{\theta} = \frac{1}{\psi - 1}\ln\psi, \tag{B4}$$

where $\psi \equiv \rho_w c_w \theta/m$ (Taylor, 1941). The momentum per unit area I_{trans} transmitted into the plate up to the instant of cavitation is given by

$$I_{trans} = I_0\zeta, \tag{B5}$$

where $\zeta \equiv \psi^{\psi/(1-\psi)}$.

References

Balden, V.H., Nurick, G.N., 2005. Numerical simulation of the post-failure motion of steel plates subjected to blast loading. International Journal of Impact Engineering 32, 14–34.

Deshpande, V.S., Heaver, A., Fleck, N.A., 2006. An underwater shock simulator. Proceedings of the Royal Society A 462, 1021–1041.

Fleck, N.A., Deshpande, V.S., 2004. The resistance of clamped sandwich beams to shock loading. Journal of Applied Mechanics 71 (3), 386–401.

Florence, A.L., 1966. Circular plate under a uniformly distributed impulse. International Journal of Solids and Structures 2, 37–47.

Guduru, P.R., Freund, L.B., 2002. The dynamics of multiple neck formation and fragmentation in high rate extension of ductile materials. International Journal of Solids and Structures 39, 5615–5632.

Guduru, P.R., Bharathi, M.S., Freund, L.B., 2006. The influence of a surface coating on the high-rate fragmentation of a ductile material. International Journal of Fracture 137, 89–108.

Hutchinson, J.W., Neale, K.W., 1977. Influence of strain-rate sensitivity on necking under uniaxial tension. Acta Metallurgica 25, 839–846.

Kazemahvazi, S., Radford, D.D., Deshpande, V.S., Fleck, N.A., 2007. Dynamic failure of clamped circular plates subjected to an underwater shock. Journal of Mechanics of Materials and Structures 2 (10), 2007–2023.
Lee, Y.-W., Wierzbicki, T., 2005a. Fracture prediction of thin plates under localized impulsive loading. Part I: dishing. International Journal of Impact Engineering 31, 1253–1276.
Lee, Y.-W., Wierzbicki, T., 2005b. Fracture prediction of thin plates under localized impulsive loading. Part II: discing and petalling. International Journal of Impact Engineering 31, 1277–1308.
Menkes, S.V., Opat, H.J., 1973. Tearing and shear failure in explosively loaded clamped beams. Experimental Mechanics 13, 480–486.
Nurick, G.N., Shave, G.C., 1996. The deformation and tearing of thin square plates subjected to impulsive loads—an experimental study. International Journal of Impact Engineering 18 (1), 99–116.
Qiu, X., Deshpande, V.S., Fleck, N.A., 2005. Impulsive loading of clamped monolithic and sandwich beams over a central patch. Journal of the Mechanics and Physics of Solids 53, 1015–1046.
Shenoy, V.B., Freund, L.B., 1999. Necking bifurcations during high strain rate extension. Journal of the Mechanics and Physics of Solids 47, 2209–2233.
Taylor, G.I. 1941. The pressure and impulse of submarine explosion waves on plates. The Scientific Papers of G.I. Taylor, vol. III, 1963. Cambridge University Press, Cambridge, pp. 287–303.
Tvergaard, V., 1993. Necking in tensile bars with rectangular cross-section. Computer Methods in Applied Mechanics and Engineering 193, 273–290.
Wang, A.J., Hopkins, H.G., 1954. On the plastic deformation of built-in circular plates under impulsive load. Journal of the Mechanics and Physics of Solids 3, 22–37.
Xue, Z., Hutchinson, J.W., 2007. Neck retardation and enhanced energy absorption in metal-elastomer bilayers. Mechanics of Materials 39, 473–487.